# Calculated electronic structure of $Pb_{1-x}Mn_xTe$ ($0 \leqslant x < 11\%$): The role of $L$ and $\Sigma$ valence band maxima

A. Łusakowski
*Institute of Physics, Polish Academy of Sciences, Al. Lotników 32/46, 02-668 Warsaw, Poland*

P. Bogusławski
*Institute of Physics, Polish Academy of Sciences, Al. Lotników 32/46, 02-668 Warsaw, Poland and*
*Institute of Physics, University of Bydgoszcz, ul. Chodkiewicza 30, 85-072 Bydgoszcz, Poland*

T. Radzyński
*Institute of Physics, Polish Academy of Sciences, Al. Lotników 32/46, 02-668 Warsaw, Poland*
(Received 10 November 2010; revised manuscript received 28 January 2011; published 24 March 2011)

Density functional theory (DFT) calculations of the electronic structure of $Pb_{1-x}Mn_xTe$ were performed using the OPENMX package with fully relativistic pseudopotentials. Because of the underestimation of the band gap in DFT, "bare" DFT calculations give a wrong order of bands at the $L$ point. Correct band structures of both PbTe and $Pb_{1-x}Mn_xTe$ as well as correct pressure coefficients of the fundamental gap are obtained by tuning the strength of the spin-orbit coupling for $6p$(Pb) orbitals. The results confirm the critical role of the valence band maximum at the $\Sigma$ point in the transport properties of $p$-PbTe and $p$-$Pb_{1-x}Mn_xTe$. With the increasing content of Mn in $Pb_{1-x}Mn_xTe$ the band gap at $L$ increases while the indirect $L$-$\Sigma$ band decreases. The energies of $L$ and $\Sigma$ maxima are equal for 9% of Mn. These results confirm previous empirical interpretations of experimental data. The role of internal distortions due to the lattice mismatch and the influence of Mn on spin properties of free carriers are analyzed.

DOI: 10.1103/PhysRevB.83.115206 PACS number(s): 71.15.Mb, 71.20.Nr, 71.70.Gm

## I. INTRODUCTION

Lead chalcogenides PbS, PbSe, and PbTe are narrow gap semiconductors with the low temperature direct gap $E_g =$ 0.29, 0.17, and 0.19 eV, respectively, which is situated at the $L$ point of the Brillouin zone (BZ). They crystallize in the rock salt structure. The importance of these materials stems from their applications in the infrared detectors and lasers.[1] Lead chalcogenides are also used in thermoelectric applications.[2–4] A recent significant advancement was the demonstration that the thermoelectric power of $Pb_{1-x}Mn_xTe$ mixed crystals containing 5–10 atomic percent of manganese is about twice higher than that of pure PbTe.[5]

The overall band structure of lead chalcogenides is well described by the local density approximation (LDA) to the density functional theory.[6–11] However, the well-known LDA underestimation of the fundamental band gap leads to an erroneous "inverted" order of bands at the $L$ point since the energies of the bottom of the conduction band (CBB) and of the top of the valence band (VBT) are interchanged. These states have the $L_6^-$ and $L_6^+$ symmetries, respectively, where the sign reflects their parity (the origin is fixed at the cation site). The wrong band order results, in particular, in the wrong, (i.e., positive) sign of the pressure coefficient of the band gap. $GW$ calculations[10] or the use of hybrid functionals[12] provide correct results. The correct results were also obtained after a rigid upward shift of the conduction band employed in Ref. 6.

An important feature of the PbTe band structure is the presence of 12 equivalent secondary maxima of the valence band located at the $\Sigma$ direction, close to the middle between the $\Gamma$ and $K$ points. Energetic proximity of the maxima at $\Sigma$ and $L$ was first evidenced by early calculations of Lin and Kleinman,[13] and subsequently confirmed by recent results.[10] The presence of the $\Sigma$ maxima does not influence appreciably optical properties of chalcogenides, such as luminescence, because the $\Sigma$-$L$ gap is indirect, and the maxima at $\Sigma$ were not discussed in previous theoretical *ab initio* works. On the other hand, a number of properties in IV-VI crystals such as thermoelectricity[5] or magnetic interaction between magnetic ions in PbTe (Ref. 14), are affected by the $\Sigma$ band. Properties of PbTe are reviewed in Ref. 15, where, in particular, the role of the $\Sigma$ band is discussed.

Experimentally, at zero temperature the secondary $\Sigma$ maximum is about 0.2 eV lower in energy than the main $L_6^+$ maximum. With the increasing temperature the fundamental gap at the $L$ point increases while the energy of the indirect $L$-$\Sigma$ gap is almost constant (i.e., the $\Sigma$ maximum moves up with respect to the top of the valence band at $L$ Ref. 5). Accordingly, transport measurements reveal that the role of the $\Sigma$ maximum is significant, or even dominant, at high temperatures and at high concentrations of holes. This is due to the effective mass of the holes in the $\Sigma$ maximum and the corresponding density of states being higher than those at $L$. Considering $Pb_{1-x}Mn_xTe$ the dependence of the band structure on the Mn content was studied by Vinogradova *et al.*[16] The results were applied to PbSnMnTe (Ref. 17) and PbMnTe (Ref. 5) in the context of thermoelectric properties. From Refs. 5 and 17 it follows that a consistent interpretation of experiment is obtained within a model in which the changes of the band structure of PbTe upon addition of Mn and upon temperature increase are similar. According to this model, the energy gap at the $L$ point increases with $x$ as $E_g = 0.19 + 2.5x$ eV. A similar influence of Mn on the band gap is found for PbMnSe (Ref. 18). The second effect induced by the presence of Mn

 

is the increase of energy of the Σ maximum relative to the top of the valence band at $L$. For Mn concentrations higher than $x \approx 0.09$ the maximum at Σ is higher in energy than the maximum at $L$, and thus the fundamental band gap of $Pb_{1-x}Mn_xTe$ is indirect. This profound modification of the valence band structure affects characteristics of free holes and thus the thermoelectric properties of $p$-PbMnTe.

Optimization of thermoelectric properties of $Pb_{1-x}Mn_xTe$ aimed at applications requires understanding the influence of manganese ions on the band structure,[19] which is the goal of this work. The calculations were performed using LDA. As it was mentioned, LDA leads to the "inverted band structure" with a wrong order of bands at $L$, which is a combined result of the too small LDA band gap and the large spin-orbit splitting. In fact, because the elements constituting the $Pb_{1-x}Mn_xTe$ alloy, especially Pb, are heavy, the spin–orbit interaction and other relativistic effects must be included. This was done using the OPENMX package.[20] In Sec. III we show that by reducing the spin-orbit (S-O) coupling of Pb the correct band structure of pure PbTe is obtained within LDA. The composition dependence of the electronic structure of $Pb_{1-x}Mn_xTe$ is analyzed in Sec. IV, and our results fully support the model of Ref. 5. We also discuss the influence of the Mn spin on the band structure of $Pb_{1-x}Mn_xTe$. Section V concludes the paper.

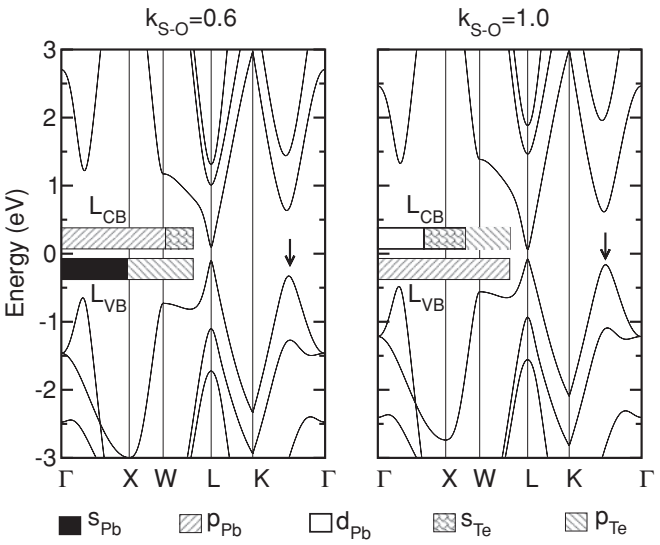


FIG. 1. PbTe band structure for two different strength of the spin-orbit coupling for Pb $6p$ electrons, see text, and a two-atom primitive cell. Note that the two band structures are almost identical. The Σ maxima are denoted by arrows. The horizontal bars schematically show the contributions of different atomic orbitals to the wave functions at the L point for valence (VB) and conduction (CB) bands.

## II. METHOD OF CALCULATIONS

*Ab initio* calculations were done using Ceperly-Alder[21] LDA exchange-correlation functional. We used the open-source OPENMX package for DFT calculations.[20] The package includes fully relativistic pseudopotentials. In addition, the package contains the program ADPACK to generate pseudopotentials with the demanded number of valence electrons. The original pseudopotentials distributed with OPENMX were generated assuming a large number of valence electrons for both Pb and Te (20 and 16 electrons, respectively). Because of the large size of our supercells it was important from the computational point of view to use pseudopotentials with lower numbers of valence electrons. Consequently, we generated fully relativistic pseudopotentials with $6s^26p^2$ and $5s^25p^4$ configurations for Pb and Te (i.e., with four and six valence electrons, respectively). The pseudopotentials were calculated using the Troullier-Martins[22] algorithm with Kleinmann-Bylander factorization.[23] For Pb, for unbound states Hamann scheme[24] was used. For Pb the cutoff radii for $6s$, $6p$, $6d$, and $6f$ pseudopotentials were 1.90, 2.48, 3.50, and 3.50 atomic units (a.u.), respectively. For Te the cutoff radii were 2.40 and 2.20 a.u. for $5s$ and $5p$ pseudopotentials, respectively. The radial cutoff for pseudoatomic orbitals for all elements was 8 a.u. In the calculations, for Te we used minimal wave functions basis (i.e., $s1p1$ in the notation explained in Refs. 25 and 26). It means that in the wave function basis for each Te atom one $s$ and three $p$ orbitals ($p_x$, $p_y$, and $p_z$) were included. The number of orbitals was doubled due to the electron's spin. For Pb the basis was $s1p1d1$, in addition to the minimal eight spinorbitals basis $s1p1$ ten $d$ spinorbitals were included. Such input parameters for pseudopotential's generation and the choice of basis set for Pb and Te leads to equilibrium lattice constant $a_{th} = 6.42$ Å for PbTe, close to the experimental value $a_{\text{exp}} = 6.46$ Å (Ref. 27). The resulting band structure is shown in Fig. 1 (left panel, $k_{S\text{-}O} = 0.6$). Since the number of Mn atoms in the supercells ranges from one to 12 it is relatively small, we used Mn pseudopotentials distributed with OPENMX with 15 valence electrons ($3s^23p^63d^54s^2$ configuration). The pseudoatomic basis for Mn was taken as $s3p2d1$. In the case of spin-polarized calculations for $Pb_{1-x}Mn_xTe$ the initial spin configuration is defined in the input, and then it is allowed to change in the process of reaching self-consistency. Importantly, OPENMX enables also to calculate pseudopotentials with a varying strength of the S-O coupling for electrons on various shells. This possibility will be exploited in Sec. III to adjust the theoretical band gap of PbTe to the experimental value.

Properties of $Pb_{1-x}Mn_xTe$ were calculated with $3 \times 3 \times 3$ simple cubic supercells containing 216 atoms. Thus, one Mn atom in the supercell corresponds approximately to the Mn content $x = 0.00926$ in $Pb_{1-x}Mn_xTe$. We used 80 Ry as the cutoff energy and $2 \times 2 \times 2$ $k$-point grid for the Brillouin zone summations. As we checked, a higher cutoff energy, 100 Ry, and a denser $4 \times 4 \times 4$ $k$-point grid does not lead to distinguishable changes of band energies. Finally, we point out that the $3 \times 3 \times 3$ supercell as well as its Brillouin zone are simple cubic. Calculations of supercell energy bands were performed along the Γ-$X$-$R$-$M$-Γ path, where the $R$ and $M$ points ($R$ is the vertex of the cube, $M$ lies in the middle of cube's edge) correspond, respectively, to the $L$ and $K$ points in the Brillouin zone of the NaCl lattice. Thus, for example, the Σ direction between Γ and $K$ in the rock salt structure corresponds to the Γ-$M$ direction in the simple cubic geometry. In the following, while presenting and discussing results for PbMnTe we denote the primary and secondary bands by $L$ and Σ, respectively, since such a notation is more natural.

In the calculations the experimental lattice constants of $Pb_{1-x}Mn_xTe$ were assumed. The measured decrease of the lattice constant due to the doping with Mn is relatively small, and amounts to 0.00632 Å per one atomic percent of Mn (Ref. 28).

## III. BAND STRUCTURE OF PbTe

The direct energy gap of PbTe amounts to 0.19 eV and is located at the $L$ point of the Brillouin zone. In the vicinity of $L$ the wave functions of the valence and the conduction bands consist of tellurium $5p$ and lead $6p$ orbitals, respectively. As it was mentioned in the Introduction, LDA provides the inverted order of bands when S-O interaction is included. In the previous work[27] we showed that the correct order of levels and the band gap value can be restored by properly reducing the strength of S-O interaction for Pb $6p$ orbitals. The strength is controlled by the parameter $k_{S\text{-}O}$ that varies from 0 to 1. $k_{S\text{-}O} = 0$ corresponds to the neglect of the S-O coupling, and $k_{S\text{-}O} = 1$ corresponds to the S-O interaction resulting from the solution of the Dirac equation for Pb atom.

In Fig. 1 we compare the calculated band structures of PbTe for two different strengths of S-O coupling. The two band structures are almost identical. However, the inspection of the wave function in the vicinity of $L$ shows that in the case of $k_{S\text{-}O} = 1.0$ (right panel) the order of bands is wrong: The wave function of the top of the valence band consists of Pb $6p$ orbitals, while that of the conduction band bottom is built from Te $5s$, Te $5p$, and Pb $6d$ orbitals, as it is shown in Fig. 1. This erroneous result is due to the fact that the S-O interaction splits both Pb and Te $p$ states, and the strength of the splitting is so large that it renders the energy of $6p$ (Pb) orbitals below energy of $5p$ (Te) orbitals.

The correct band structure obtained by reducing the S-O coupling of Pb by 40% is shown in the left panel of Fig. 1, and is denoted as $k_{S\text{-}O} = 0.6$. While the band structures obtained with $k_{S\text{-}O} = 1$ and $k_{S\text{-}O} = 0.6$ are very similar, the proper order of levels at $L$ and the correct sign of the gap pressure coefficients is obtained only with $k_{S\text{-}O} = 0.6$. With this choice the results agree very well with those of Refs. 10 and 11. In particular, the energy of the $\Sigma$ maximum is 0.25 eV below that at $L$, which is in good agreement with the result of the quasiparticle self-consistent $GW$ approximation,[10] 0.21 eV. Next, the present calculations show that for the lattice constant in the interval $a = 6.3$–$6.6$ Å the energy gap changes linearly with $dE_g/da \approx 0.8$ eV/Å. Thus, the deformation potential $C$ defined by $\Delta E_g = C\epsilon$, where the strain $\epsilon = \Delta a/a$, is $C = 5.2$ eV, which is close to the result of Ref. 10.

The calculated energy levels at $L$ are schematically shown in Fig. 2, where $L_6^+$ and $L_6^-$ states are denoted, respectively, as $L_{\text{val}}$ and $L_{\text{cond}}$. The figure also explains the change of sign of the gap pressure coefficient. As it follows from the calculations, with the increasing pressure the energy of the $L_{\text{val}}$ level relative to $L_{\text{cond}}$ increases, which closes the gap for the correct order (Fig. 1, $k_{S\text{-}O} = 0.6$), and opens the gap for the inverted order of bands. We stress that the proper order of bands at the $L$ point in PbTe is critical to obtain not only the correct pressure coefficients of the band gap, but also a correct composition dependence of $Pb_{1-x}Mn_xTe$ alloy discussed in the next section. Although the main interest in this work is

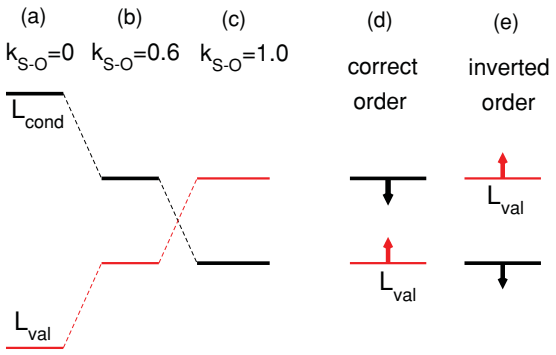


FIG. 2. (Color online) (a)–(c) The dependence of bands' order on the spin-orbit coupling strength. Motion of the bands' extrema induced by external pressure for the (d) correct and the (e) inverted bands' order.

PbMnTe, we mention that the same effect was obtained for PbCdTe: Pseudopotentials that fully include the S-O coupling and lead to the inverted band structure for PbTe result in the decrease of the energy gap with the increasing Cd content, in contrast to the experiment.

## IV. ELECTRONIC STRUCTURE OF PbMnTe

### A. Dependence of the band gaps on the chemical composition

The calculated band structure of $Pb_{1-x}Mn_xTe$ is shown in Fig. 3 for the Mn content increasing from 0 to about 11%, (i.e., from 0 to 12 Mn ions in the supercell). One can see that the $\Sigma$ maximum of the valence band of pure PbTe does not fold exactly to the $\Gamma$ point of the supercell (i.e., it is situated off the center between $\Gamma$ and $M$). This is also the case for two Mn ions in the supercell, although the maximum is very close the $\Gamma$ point. For higher concentration of Mn the maximum is situated at $\Gamma$. The energy gap at the $R$ point (which corresponds to the $L$ point in the rock salt structure) increases with an average slope of about 15 meV per atomic percent of Mn. In parallel, the energy of the secondary minimum at $\Sigma$ (folded to the $\Gamma$ point) increases as well, and the energies of the two minima coincide for $x \approx 0.09$. The results are summarized in Fig. 4 (filled symbols), which shows the calculated direct $L$-$L$ and indirect $L$-$\Sigma$ gaps.

The obtained results indicate that the dependence of $E_g$ on the composition may be somewhat nonlinear, but the effect is small. In fact, one should note that in the supercell method the precise value of the gap of an alloy can depend on the detailed distribution of Mn ions in the supercell. To verify the role of this factor the calculations were performed for several Mn configurations. Energy bands obtained for three configurations are shown in Fig. 5. From these and other results it follows that the gap typically spans the energy window of about 0.04 eV, only in the case of six Mn in the supercell we found configurations for which the differences in the energy gap were about 0.1 eV. In Fig. 4 the average values are shown.

To show separately the effects of the change of the chemical composition and those of the change of the lattice constant, in Fig. 4 we also present the results of calculations for the lattice constant fixed to $a = 6.46$ Å to that of pure PbTe for all $x$ (open symbols). As it was mentioned, the addition

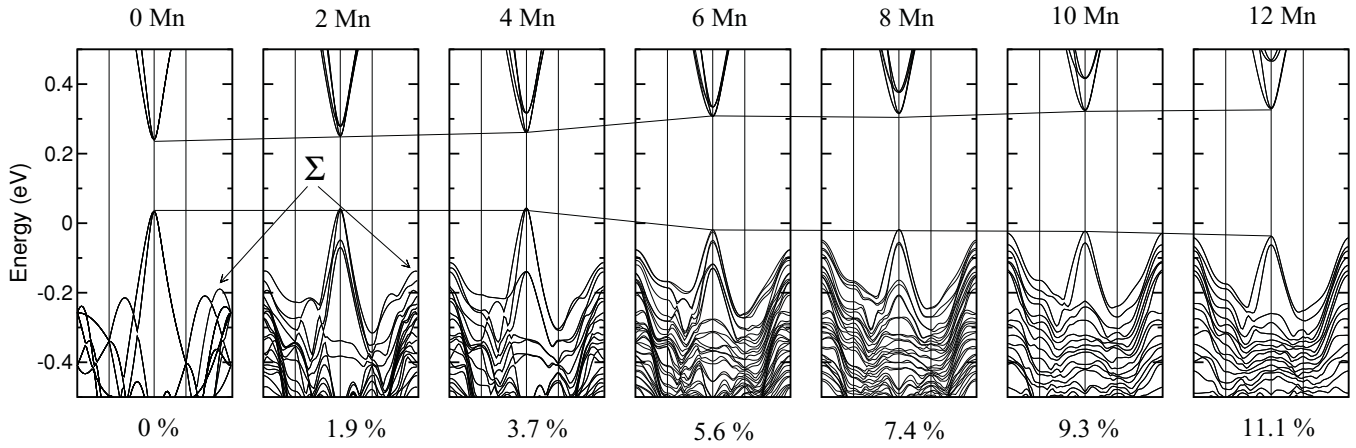


FIG. 3. Energy bands along the Γ-*X*-*R*-*M*-Γ path for 216-atom supercells containing from 0 to 12 Mn atoms. The *R* point of the supercell Brillouin zone corresponds to the *L* point of the rock salt PbTe. The lines connecting band extrema at *R* are for the eye guide. For the two lowest Mn concentrations we show positions of the bands corresponding to Σ band in the rock salt lattice. For higher Mn concentrations the top of this band is at the Γ point.

of Mn reduces the lattice constant. This, in turn, leads to the reduction of $E_g$ seen in the figure. This reduction is given by the calculated deformation potential of pure PbTe to a very good approximation, which shows that the deformation potential of the band gap of $Pb_{1-x}Mn_xTe$ practically does not depend on the Mn content.

The obtained agreement with the experiment is satisfactory. First, the calculated direct gap at *L* increases with the Mn content. The calculated slope of 15 meV per atomic percent of Mn is somewhat smaller than the experimental value, 25 meV per atomic percent of Mn (Ref. 5). Second, the measured energies of the *L* and Σ maxima are equal for $x \approx 9\%$ (Ref. 29), in full agreement with the present results. Finally, the indirect Σ-*L* gap is almost independent on the composition.[29]

It should be observed that a direct comparison of theoretical results with experimental data for high Mn contents may not be straightforward because of the possible microscopic nonuniformity of the Mn distribution. In fact, in typical alloys of semiconductor compounds the chemically mixed sublattice contains atoms from the same group of the Periodic Table. This is not the case of PbMnTe, where group-II Mn substitutes group-IV Pb. Moreover, the end compounds, PbTe and MnTe, crystallize in different structures. As a result, the rock salt structure of PbTe becomes unstable with the increasing Mn content, and the formation of both the composition fluctuations and inclusions of second phase is expected. Both effects occur in GaMnAs (Ref. 30). These factors affect the electronic structure.

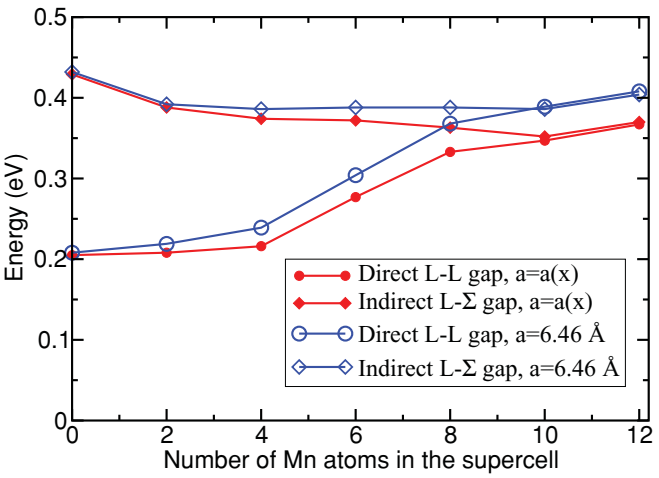


FIG. 4. (Color online) Dependencies of the direct *L*-*L* (circles) and indirect *L*-Σ (diamonds) energy gaps on number of Mn atoms in the supercell. Filled points—energy gaps for Mn-dependent lattice constant, open points—for the lattice constant fixed to 6.46 Å.

### B. Effects of internal distortions

The calculated band structure depends on the microscopic distortions of the $Pb_{1-x}Mn_xTe$ alloy. They stem from the fact that the ionic radius of Mn is smaller than that of Pb. We performed geometry optimization for $2 \times 2 \times 2$ supercell containing one Mn atom placed in the supercell's center. In the procedure all internal atoms in the supercell, except the Mn atom, were allowed to move, while the positions of atoms

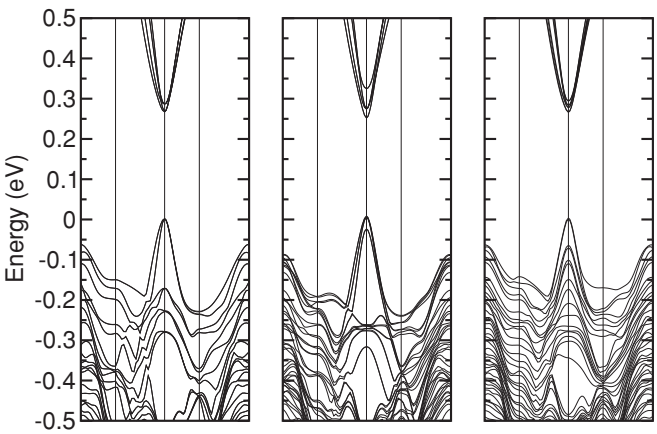


FIG. 5. PbMnTe band structure along Γ-*X*-*R*-*M*-Γ path for three different distributions of four Mn atoms in the 216 atom supercell.

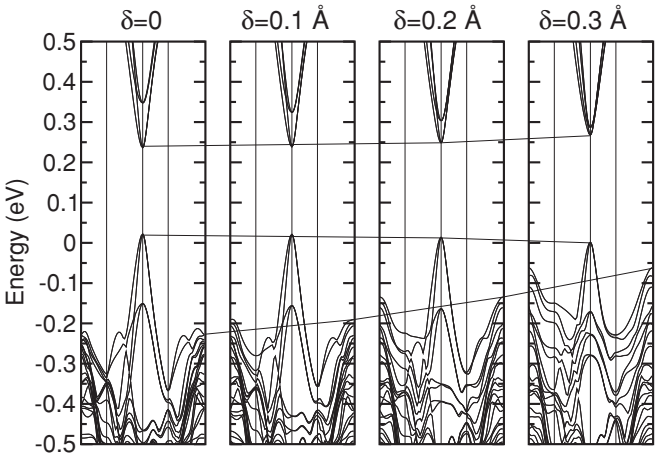


FIG. 6. Dependence of the electronic band structure along the Γ-*X*-*R*-*M*-Γ path for 216 atom supercells containing four Mn atoms on the deformation $\delta$. The lines connecting tops of the bands are for eye guide.

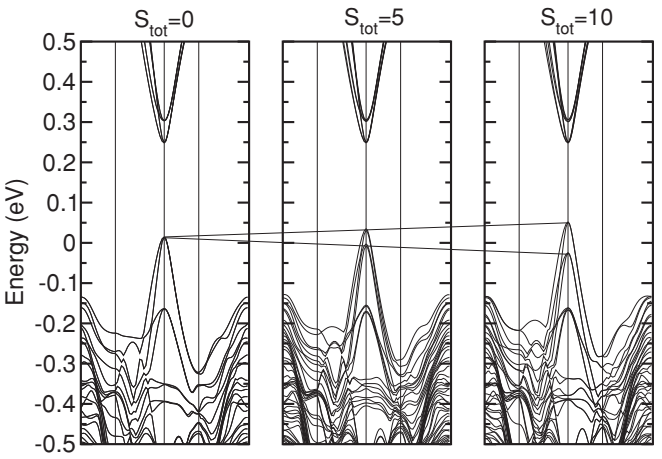


FIG. 7. Dependence of the electronic band structure along Γ-*X*-*R*-*M*-Γ path for 216 atom supercells containing four Mn atoms on their total spin. The lines connecting tops of the bands are for eye guide.

placed on the supercell's faces were fixed. The results of the geometry optimization show that after replacing Pb by Mn the main effect consists in a displacement $\delta$ of about 0.2 Å of the six nearest Te neighbors toward the central Mn ion. In the band structure calculations $\delta = 0.2$ Å was assumed. Positions of more distant ions also change, but the displacements are more than an order of magnitude smaller. These results are in agreement with the extended x-ray absorption fine structure (EXAFS) measurements[31] performed for SnMnTe. They show that the average distance between Mn and Te is about 2.95 Å, and one expects that the Mn-Te distance in PbMnTe is close to this value. On the other hand, the Pb-Te distance in PbTe is 3.23 Å.

The calculated dependence of the energy bands on $\delta$ is shown in Fig. 6. In this case, the values of the distortion $\delta$ are fixed in the input, and the atoms are not allowed to relax. With the increasing $\delta$ both the increase of the direct gap at $L$, and the stronger decrease of the indirect $L$-Σ gap, are seen. Using a higher $\delta = 0.3$ Å we find that the energy gap at $L$ increases by 22 meV per Mn atomic percent, and the Σ band becomes the principal band for smaller Mn content, $x = 0.05$. The data presented in Fig. 6 demonstrate that the increase of $Pb_{1-x}Mn_xTe$ band gap with the increasing Mn content is largely due to the microscopic deformations. Interestingly, a similar effect of the strong lattice mismatch (i.e., the change of the band gap upon addition of ions with a much smaller radius) is found for GaAs:N (Ref. 32) for small N concentrations. In both alloys the effect can be interpreted as a consequence of the dilatation of the host lattice by the small atoms. However, in GaAs and PbTe the effect has the opposite sign due to the opposite sign of the band gap pressure coefficients: in GaAs, dilatation closes the gap, while in PbTe it opens the gap.

### C. Effects of the spin polarization

The band structures shown in Fig. 3 were obtained assuming a configuration of Mn spins with the total spin $S_{tot} = 0$. This corresponds to the experimental situation of the vanishing magnetic field. The dependence of the energy bands on magnetization is shown in Fig. 7 for the 216-atom cell with four Mn ions (i.e., $x = 0.037$) and the total spin $S_{tot}$ equal to 0, 5 and 10. The coupling between Mn ions, which are relatively distant in the considered configuration, is weakly antiferromagnetic and the $S_{tot} = 0$ state is lower in energy by about 5 meV then that with $S_{tot} = 10$. A detailed study of the magnetic Mn-Mn coupling in PbTe is outside the scope of this work.

The linear increase in spin splitting of the top of the $L$ valence band with the increasing magnetization is clearly seen. The much smaller splitting of the conduction band is not seen in the scale of the picture.

In PbMnTe, there are four exchange integrals, $\alpha$, $\beta_\perp$, $\beta_\parallel$, and $\delta$, which characterize influence of the magnetic ions on the band structure. From the experimental point of view there are two exchange constants describing splitting: $A$ for holes and $B$ for electrons. These constants are combinations of $\alpha$, $\beta_\perp$, $\beta_\parallel$, and $\delta$ with coefficients characterizing spin-orbit mixing in PbTe, and definitions are given in Ref. 33. The splittings of the top of the valence band and the bottom of the conduction band are $\Delta E_v = A\langle S\rangle x$ and $\Delta E_c = B\langle S\rangle x$, respectively, where $\langle S\rangle = 5/2$ is the average Mn spin length. For $S_{tot} = 10$, the calculated splittings of the valence and of the conduction bands at the $R$ point are 0.076 and 0.002 eV, respectively. The hole-Mn coupling is antiferromagnetic, while the electron-Mn coupling is ferromagnetic. Using these values we obtain $A = 0.86$ eV and $B = 0.02$ eV, while the experimental values are $A_{exp} = 0.18$ eV and $B_{exp} = 0.03$ eV (Ref. 33), and both integrals are of antiferromagnetic sign. The calculated hole-Mn exchange integral is of proper sign and of proper order of magnitude, although the value is too large. A similar overestimation of the $p$-$d$ coupling is found for GaMnAs (Ref. 34). On the other hand, although the calculated absolute value of the constant $B$ is comparable to the experimental one, the sign of the integral is wrong. However, we stress that the accuracy of the calculations, about 2 meV, is close to the splitting energy, a thus a detailed discussion of $B$ is not justified.

Analysis of the mechanisms leading to the *sp-d* exchange coupling in PbMnTe was performed by Dietl *et al.*[35] In this work the authors considered two main contribution: the so-called kinetic exchange and direct exchange. The kinetic exchange is due to hybridization between 3*d* shell of Mn and the orbitals of surrounding ions, and leads to the antiferromagnetic sign of the *sp-d* interaction. The second mechanism, the direct exchange, which is always of ferromagnetic type, is due to internal exchange interaction between 3*d* electrons of manganese and the electrons on its nonmagnetic 4*s* and 4*p* orbitals. These nonmagnetic orbitals contribute to the valence and conduction states, and in this way the direct intraatomic exchange contributes to the band spin splitting. The top of the valence band is built mainly from *p*(Te) orbitals, and Te ions are the nearest neighbors of Mn. Thus, the hybridization between *p*(Te) and *d*(Mn) is strong, and so is the impact of the magnetic ordering of Mn on the free holes. On the other hand, the bottom of the conduction band is mainly built from the *p*(Pb) states, Pb ions are second neighbors of Mn, and thus the *p*(Pb)-*d*(Mn) hybridization is weak. Spin splitting of the valence band at $L$ increases when the Mn-Te distance becomes smaller, (i.e., it increases with the increasing distortion $\delta$), while the spin splitting of the conduction band remains the same. For $\delta = 0.3$ Å the valence band splitting increases to 0.1 eV and the conduction band splitting remains 0.002 eV.

## V. CONCLUSION

In conclusion, we performed *ab initio* calculations of the band structure of PbMnTe. We showed that reducing the spin-orbit strength for Pb 6*p* electrons by approximately 40% leads to the correct electronic structure of PbTe. In particular, this approach reproduces the correct order of bands at $L$, the value of the band gap and of its pressure coefficient, and the presence of the secondary $\Sigma$ valence band maximum at about 0.2 eV below the valence band top at $L$. Of particular interest for this work is the $\Sigma$ maximum because it is close in energy to the maximum at $L$ and it plays an important role in the transport properties in *p*-type samples. The calculated dependence of band structure of PbMnTe on the Mn content agrees with the experimental data and confirms the empirical model proposed in Ref. 5. With the increasing Mn content the direct gap at $L$ increases and the indirect $\Sigma$-$L$ gap decreases. The energies of the $\Sigma$ and $L$ valence band maxima are equal for $x \approx 0.09$, which is very close to the experimental value. The calculated increase of the band gap at $L$ is 0.015 eV per atomic percent of Mn, again in close agreement with the experimental value of 0.025 eV. The opening of the gap at $L$ and, in particular, relative motion of the $\Sigma$ and $L$ bands are largely due to the microscopic distortions of the lattice around the Mn ions induced by the misfit of Pb and Mn atomic radii. We also discussed the influence of total manganese spin on the band structure and estimated the exchange constants between Mn and free carriers.

## ACKNOWLEDGMENTS

This work was partially supported by the European Union within the European Regional Development Fund, through the Innovative Economy Grant No. POIG.01.01.02-00-108/09 and by the US Army Research Office under Contract/Grant No. W911NF-08-1-0231. We thank T. Story for the critical reading of manuscript.

[1] H. Zogg and A. Ishida in *Infrared Detectors and Emitters: Materials and Devices*, edited by P. Capper and C. T. Elliott (Kluwer Academic Publishers, Dordrecht, 2001).
[2] G. Chen, M. S. Dresselhaus, G. Dresselhaus, G. Fleurial, and T. Caillat, Inte. Mater. Rev. **48**, 45 (2003).
[3] J. P. Heremans, V. Jovovic, E. S. Toberer, A. Saramat, K. Kurosaki, A. Charoenphakdee, S. Yamanaka, and G. J. Snyder, Science **321**, 554 (2008).
[4] G. J. Snyder and E. S. Toberer, Nat. Mat. **7**, 105 (2008).
[5] V. Osinniy, A. Jędrzejczak, W. Domuchowski, K. Dybko, B. Witkowska, and T. Story, Acta Phys. Pol. A **108**, 809 (2005).
[6] S. H. Wei and A. Zunger, Phys. Rev. B **55**, 13605 (1997).
[7] K. Hoang and S. D. Mahanti, Phys. Rev. B **78**, 085111 (2008).
[8] A. Gruneis, K. Hummer, M. Marsman, and G. Kresse, Phys. Rev. B **78**, 165103 (2008).
[9] K. Hummer, A. Grüneis, and G. Kresse, Phys. Rev. B **75**, 195211 (2007).
[10] A. Svane, N. E. Christensen, M. Cardona, A. N. Chantis, M. van Schilfgaarde, and T. Kotani, Phys. Rev. B **81**, 245120 (2010).
[11] Yi Zhang, Xuezhi Ke, Changfeng Chen, J. Yang, and P. R. C. Kent, Phys. Rev. B **80**, 024304 (2009).
[12] J. Heyd, G. E. Scuseria, and M. Ernzerhof, J. Chem. Phys. **118**, 8207 (2003).
[13] P. J. Lin and L. Kleinman, Phys. Rev. **142**, 478 (1966).
[14] T. Story, P. J. T. Eggenkamp, C. H. W. Swuste, H. J. M. Swagten, W. J. M. de Jonge, and L. F. Lemmens, Phys. Rev. B **45**, 1660 (1992).
[15] *Lead chalcogenides: physics and applications*, edited by D. Khokhlov (Taylor & Francis, London, 2003).
[16] M. N. Vinogradova, I. A. Drabkin, Y. Y. Eliseeva, and I. V. Nelson, Fiz. Tekh. Poluprovodn. **6**, 1478 (1972) [Sov. Phys.-Semicond. (English Transl.) **6**, 1283 (1973)]
[17] P. Lazarczyk, M. V. Radchenko, G. V. Lashkarev, T. Story, K. Dybko, and R. R. Galazka, Semicond. Sci. Tech. **13**, 989 (1998).
[18] H. Krenn, S. Yuan, N. Frank, and G. Bauer, Phys. Rev. B **57**, 2393 (1998).
[19] G. D. Mahan and J. O. Sofo, Proc. Natl. Acad. Sci. USA **93**, 7436 (1996).
[20] see [http://www.openmx-square.org].
[21] D. M. Ceperley and B. J. Alder, Phys. Rev. Lett. **45**, 566 (1980).
[22] N. Troullier and J. L. Martins, Phys. Rev. B **43**, 1993 (1991).
[23] L. Kleinman and D. M. Bylander, Phys. Rev. Lett. **48**, 1425 (1982).
[24] D. R. Hamann, Phys. Rev. B **40**, 2980 (1989).
[25] T. Ozaki, Phys. Rev. B **67**, 155108 (2003).

[26]T. Ozaki and H. Kino, Phys. Rev. B **69**, 195113 (2004).
[27]T. Radzyński and A. Łusakowski, Acta Phys. Pol. A **116**, 954 (2009).
[28]A. Łusakowski, A. Jedrzejczak, M. Górska, V. Osinniy, M. Arciszewska, W. Dobrowolski, V. Domukhovski, B. Witkowska, T. Story, and R. R. Gałazka, Phys. Rev. B **65**, 165206 (2002).
[29]T. Story, private communication.
[30]M. Moreno, B. Jenichen, V. Kaganer, W. Braun, A. Trampert, L. Daweritz, and K. H. Ploog, Phys. Rev. B **67**, 235206 (2003).
[31]R. J. Iwanowski, W. Paszkowicz, K. Ławniczak-Jabłońska, M. H. Heinonen, B. Witkowska, and J. Feldhaus, Chem. Phys. Lett. **336**, 226 (2001).
[32]N. Gonzalez Szwacki and P. Boguslawski, Phys. Rev. B **64**, 161201 (2001).
[33]G. Bauer, H. Pascher, and W. Zawadzki, Semicond. Sci. Technol. **7**, 203 (1992).
[34]Stefano Sanvito, Pablo Ordejon, and N. A. Hill, Phys. Rev. B **63**, 165206 (2001).
[35]T. Dietl, C. Śliwa, G. Bauer, and H. Pascher, Phys. Rev. B **49**, 2230 (1994).